Flood Characteristic and Fluid Rock Interactions of a Supercritical CO_2, Brine, Rock System: South West Hub, Western Australia

Dr Ali Saeedi: Department of Petroleum Engineering, Curtin University, Western Australia

Dr Claudio Delle Piane: CSIRO Energy, Western Australia

Dr Lionel Esteban: CSIRO Energy, Western Australia

Dr Quan Xie: Department of Petroleum Engineering, Curtin University, Western Australia

<u>Contact details of the corresponding author</u>

Name: Ali Saeedi

Address: 26 Dick Perry Avenue, Kensington, WA 6151, Australia

Tel: +61 8 9266 4988

Email: Ali.Saeedi@Curtin.edu.au

1 Abstract

Chemical and/or physical interactions between the storage rock and injected and in-situ created solutes are expected to occur during many underground CO_2 storage projects. The intensity of the reactions, however, depends on the abundance of susceptible minerals (e.g. carbonates, clays) in the pore space of the host rock. Such interactions may impact on the multiphase flow characteristics of the underground fluids-rock system over short as well as long time frames.

In this research the in-situ multiphase flow characteristics of four sandstone samples have been investigated using a set of laboratory measurements. The samples tested were taken from the Wonnerup Member of the Triassic Lesueur Sandstone which is under consideration as a storage formation in the South-West Hub CO_2 geo-sequestration site in Western Australia.

All the samples tested show favourable characteristics in terms of storage capacity in the form of residual capillary trapping with residual CO_2 saturation varying between 23% and 43%. They underwent a degree of alteration to their petrophysical characteristics which was most significantly pronounced in the case of their absolute gas permeability which showed drops of 25% to 60% in the post-flood samples. Formation damage by fines migration is proposed as a mechanism for the observed reduction in permeability. The fines are believed to have originated from the kaolinite particles present in the pore space of the samples.

2 Introduction

Geologic carbon sequestration, i.e. the storage of CO_2 into buried geologic reservoir formations, is being developed worldwide and considered as a large scale greenhouse gas mitigation technology (IPCC, 2005). In Western Australia, the Perth Basin is being investigated as a potential site for CO_2 injection due to the presence of large and relatively deeply buried saline aquifer in the proximity of industrial emitters.

The successful operation and management of industrial scale projects require, among others, accurate characterization of the injectivity of CO_2 into the reservoir rocks and of their storage potential in advance during the planning stage of the projects. Injectivity is affected by the rock properties, the nature of the fluids and the in-situ conditions at depth and a proper assessment of these variables is therefore critical for the planning of any geo-sequestration project.

The South-West CO_2 Geo-sequestration Hub project (the South-West Hub) is one of the Australian Flagship Carbon Capture and Storage Projects, a government funded initiative in partnership with major local industrial CO_2 emitters. The project aims to explore the potential of storing commercial quantities of CO_2 in a deep saline aquifer as part of a precompetitive data gathering effort. As part of the early stages of the South-West Hub project, a stratigraphic well (Harvey-1) was drilled in 2012 by the Geological Survey of Western Australia (Millar and Reeve, 2014) to confirm the stratigraphy of the area and recover core material to be tested in the laboratory (Figure 1).

The potential storage target in the South-West Hub area consists of the Triassic Lesueur Sandstone subdivided into the upper Yalgorup and the lower Wonnerup Members (Figure 1). Due to the lack of outcrops, the knowledge of the potential reservoir rocks properties is limited to the sparse available material sampled from old exploration wells (see Delle Piane et al., 2013a; Delle Piane et al., 2013b; Dillinger and Esteban, 2014 and Timms et al., 2015), the new core material extracted from the Harvey-1 well is therefore invaluable for the progress of the South-West Hub project.

Relative permeability of the underground rock-fluids system influences the injectivity and subsurface movement of CO_2 and reservoir simulations are usually used to predict the CO_2 injection capacity and plume migration at a full reservoir scale. The key parameters used to determine the multiphase (formation brine and CO_2) fluids mobility and distribution in the subsurface are relative permeability in addition to porosity and permeability of the host rock (e.g. Doughty and Pruess, 2004; Kopp et al. 2009). Whereas porosity and permeability can be readily obtained from inversion of wireline log parameters or routine laboratory measurements, relative permeability is inherently more difficult to derive and requires special experimental protocols and equipment (e.g. Muller, 2011).

Two principal approaches are used to obtain a relative permeability data from laboratory measurements: i) steady state (SS) and ii) unsteady state (USS) core flooding experiments. A SS experiment consists of a number of steps with every step consisting of simultaneous injection of the two fluids at a fixed ratio through a porous rock sample. For every ratio, the constant flow rate injection continues until saturation and differential pressure along the sample stabilise and the produced ratio equals the injected ratio (Bear, 1988; Dullien, 1992). Usually, SS experiments are very time consuming and require a long time for flow stabilization.

During USS experiments, there is no simultaneous injection of the two fluid phases and one fluid phase is displaced from the saturated core sample by injecting another fluid. Contrary to the steady-state techniques, there is only one injection step involved in an USS experiment, making this type of experiment less time consuming (Dullien, 1992; Bear, 1988).

Laboratory based studies aimed at measuring the residually trapped amount of CO_2 in brine saturated sandstones and supercritical conditions include the works of Bennion and Bachu (2005), Suekane et al. (2008), Pentland et al. (2011), Saeedi et al. (2011), Shi et al. (2011), Lu et al. (2012), Saeedi (2012), Akbarabadi and Piri (2013), Ruprecht et al. (2014), Zuo and Benson (2014), Li et al. (2015). The data available in the literature globally indicates that the saturation of residually trapped CO_2 is likely to be at least 10% of the pore volume and many rocks are capable of residual trapping at saturations between 30 and 40% of the pore volume; this is predominantly controlled by the pore scale structure of a given rock type and less by the external conditions acting on the reservoirs (Krevor et al., 2015). It is worth noting that the above figures are stated based on the statistical analysis of results from the core-scale experiments conducted in the laboratory. At the much larger field-scale, other factors such as large scale formation heterogeneities in all three directions and slower frontal displacement velocities are expected to impact on the capacity of the rocks to residually trap CO_2. The impact of such factors needs to be taken into account when upscaling the core-scale laboratory results to the full field-scale using numerical simulation modelling techniques.

The main objective of this study was to investigate the multiphase flow characteristics of the supercritical CO_2 ($scCO_2$)-brine-rock system pertinent to the South-West Hub project. Four core-flooding experiments were conducted under reservoir conditions on four representative plugs sampled from the core material recovered from the Harvey-1 well. All four core-plugs belonged to the Wonnerup Member of the Lesueur Formation and were chosen as characteristic of the lithofacies type likely to represent the injection target (for details on lithofacies characteristics see Delle Piane et al., 2013b; Olierook et al., 2014 and Timms et al., 2015). The core-flooding experiments were performed using a conventional USS procedure (as briefly described earlier) with the main focus of obtaining the relative permeabilities and residual saturations.

In addition to the main core-flooding experiments, a number of auxiliary petrophysical measurements were also carried out on the samples before and after the floods (e.g. helium porosity-permeability and pore body size distribution converted from relaxation time T2 spectra by low field nuclear magnetic resonance (NMR) measurements). The purpose of these complementary measurements was to investigate any potential alterations of the petrophysical properties of the samples induced by the flooding procedure.

3 Experimental Measurements

3.1 Material and initial sample characterisation

Four horizontal (i.e. cored perpendicular to the whole-core axis) core-plugs were selected from the cored sections of Harvey-1 at depths considered relevant to the injection operations in the proposed

South-West Hub. The samples belonged to the lithofacies type of the Wonnerup Member of the Triassic Lesueur Sandstone described as interbedded coarse to gravelly cross-bedded sandstones, deposited in high-energy river channel fill and barforms (facies Ai and Aii as described by Delle Piane et al., 2013a; Olierook et al., 2014, Timms et al., 2015).

The core plugs were drilled dry from the whole-cores recovered from well Harvey-1. Upon recovery, the whole-cores were depressurised at the well site and laid into standard core trays before being transferred to the core storage facility where core plugs were drilled dry using a 3.81 cm (1.5”) coring bit. Upon cutting and trimming, the core plugs were subjected to a core cleaning process using warm toluene and methanol in a temperature controlled Dean-Stark apparatus to remove any possible contaminants (e.g. salts, possible hydrocarbons) from the samples before they undergo any of the subsequent experimental measurements. Subsequently the samples were dried in an oven for 48 hours under a temperature of 105°C. The post-flood samples were dried and their salt residues were cleaned using an approach similar to the above but only in the last stage when gas porosity-permeability measurements were performed. From the initial saturation stage to some of the analysis performed on the post-flood samples, the plugs never underwent any dehydration to avoid salt precipitation from the brine. Therefore, NMR, brine permeability and core flooding before and after experiments were acquired with the same hydration status.

A general characterization was performed on three of the four samples (206647, 206660 and 206669) by means of X-ray diffraction (XRD), mercury injection, Helium porosity and permeability and nuclear magnetic resonance (NMR), while sample 206655 underwent helium porosity and permeability measurements only and 206669 underwent NMR on pre-flooding experiments only.

Porosity and gas permeability were measured using an automated helium porosimeter-permeameter (AP 608 from Coretest Systems Inc.) at effective stresses of 1.72, 5.2 and 32.7 MPa; at each level of pressure the measurements were repeated three times to assess their reproducibility. Brine permeability of each sample was also measured at the beginning of the core-flooding experiments under in-situ reservoir conditions using a synthetic formation brine with salinity of 30,000 ppm NaCl. This formation water salinity was chosen based on the interpretation results of the resistivity logs run in well Harvey-1 only as no representative formation water samples could be collected from the well.

X-ray tomographic (XCT) images of three of the four samples were acquired using a Toshiba Asteion medical scanner to evaluate the internal structures and the integrity of the plugs. The processed XCT images were oriented at the maximum bedding angle within each plug sample and show well developed sedimentary beds in the three plugs; these are either parallel or slightly inclined to the plugs axes (Figure 2a).

Mercury Injection Capillary Pressure curves (MICP) were acquired on cubic offcuts (with side of approximately 0.7 cm) of three of the core plugs to analyse their pore size distribution. The offcuts were cut from the core plugs after undergoing the earlier outlined cleaning procedure. The offcuts were placed in a Micromeritics Autopore IV porosimeter under vacuum and injected with mercury at about 120 increasing capillary pressure steps to a maximum pressure of 413 MPa (equivalent to 2-3 nm pore throat size).

Finally, the sample characterization was completed by low field NMR measurements conducted using a Maran 2 MHz Ultra-spectrometer (Oxford Instruments Ltd) on three core plugs (206647, 206660 and 206669) before and after flooding experiments to evaluate possible changes in porosity and pore size distribution induced by the flooding tests. For NMR measurements before the flooding experiments, the samples were brine saturated under vacuum for 48 hours and then analysed. After the flooding experiments, the brine saturated samples were reanalysed using the protocol previously applied on the same samples. Note that samples 206669 and 206655 could not be properly preserved after core flooding and the post-flood NMR was not recorded for these samples. The difference in mass between the dry and brine-saturated core-plugs was used to calculate their water-filled porosity (Water Imbibition Porosity - WIP). Also, assessment of full saturation was made by comparing the WIP to the helium porosity. Once saturated, the samples were tested in the NMR spectrometer using a Carr–Purcell–Meiboom–Gill (CPMG) pulse sequence following the protocol described in the literature (e.g. Dillinger and Esteban, 2014). This spin-echo method records the pore size distribution, similar to mercury porosimetry, using the transverse magnetic relaxation time (T_2). In an NMR test the magnetization and transverse relaxation time (T_2) of hydrogen nuclei contained in the pore fluid is measured. Different pore sizes in fluid saturated rocks will produce characteristic T_2 distributions as the amplitude of transverse magnetization is proportional to the number of hydrogen nuclei (Dunn et al., 2002). As a consequence, the observed T_2 distribution of a saturated core sample can be converted into pore size distribution of the rock using literature data transform from sandstones (Jorand et al., 2011; Kleinberg et al., 2003a; Kleinberg et al., 2003b). The Maran 2 MHz and the experimental protocol ensure a resolution of pore body size about 0.1 µm assuming that no or little amount of paramagnetic and ferromagnetic minerals, such as magnetite or metalloids, perturbate the T_2 relaxation (Nicot et al., 2006).

3.2 Core-flood Setup

Table 1 lists the pressure and temperature values used during the experiments; for each sample, the pressure, temperature and salinity values correspond to those at the depth from which the sample was recovered. The fluids used during the various stages of this experimental work consisted of deaerated dead formation brine (i.e. formation brine with no gas content), CO_2-saturated brine and water vapour-saturated scCO_2. The CO_2 gas used was of at least 99.9 mol % purity. Formation brine and CO_2 were mutually saturated with each other in a stirred Parr reactor under in-situ conditions. The formation brine was prepared in the lab using distilled water and appropriate amounts of analytical grade sodium chloride (NaCl) supplied by Sigma-Aldrich.

The experiments were carried out using a high pressure-high temperature, three-phase steady-state core-flooding apparatus. A schematic of the core-flooding rig is presented in Figure 3. Comprehensive details on the specifications of the core-flooding apparatus can be found elsewhere (Saeedi, 2012; Saeedi et al., 2011).

3.3 Core-flood Procedure

During the core-flooding experiments a specially designed multi-layered combination sleeve was used. This combination sleeve was utilised to prevent the diffusion of CO_2 which normally occurs through most conventional flexible rubber sleeves. A full description of various components of the sleeve is presented elsewhere (Saeedi et al., 2011). In order to eliminate the effect of gravity segregation (i.e. underrun or override of the injected fluids) the core-holder containing the sample was placed vertically so the injection would be performed from the base to the top. In order to apply overburden pressure to the sample, after loading the wrapped sample into the core-holder, using a hand pump, the overburden fluid was pumped slowly into the annular space of the core holder.

Below is an outline of the steps involved in carrying out the conventional USS core-flooding experiments. This procedure has been designed based on the standard procedures and protocols available in the literature (Bennion and Bachu, 2005; Izgec et al., 2008; Perrin and Benson, 2010; Saeedi et al., 2011).

1. After loading a sample into the core-holder and gradually increasing the overburden pressure to the reservoir net effective stress, low pressure CO_2 gas was passed through the sample for at least 20 minutes to displace and replace the air present in the sample's pore space. Compared to air, the CO_2, due to its small sized molecules and higher diffusivity (Baker and Low, 2014), could be evacuated from the sample more effectively when required. Furthermore, any remaining CO_2 after evacuation would readily dissolve in the saturating dead brine and removed from the sample during the later in-situ saturation and initial brine permeability measurement process.
2. After flushing the sample with CO_2, all the flow-lines and the sample inside the core-holder were vacuumed using a vacuum pump for at least 24 hours. Then the back pressure was brought to full in-situ reservoir pressure, and the air bath temperature was raised to the reservoir temperature. Then the core sample was saturated using dead formation brine while the confining pressure was increased and then maintained equal to its in-situ reservoir value. The sample was left under reservoir conditions in contact with brine for another 48 hours to become completely saturated with dead brine and to establish adsorption equilibrium. The full saturation was confirmed by the constant pressure reading from the injection pump, which maintained the pore pressure of the core sample during the above 48 hours. For some of the experimental work where the sample could be accessed during the saturation with minimum effort (e.g. core saturation for the NMR tests), the

volume of injected brine was also tracked from mass intake assuming a brine density of 1.03 g/cc and compared to pore volume from gas porosity measurements to ensure complete saturation (> 98% in all the tested plugs).

3. In the next step, the CO_2-saturated brine was injected into the core sample at constant flow-rate to displace the dead formation brine. The CO_2-saturated brine injection continued until steady-state conditions were achieved (i.e. constant and steady differential pressure across the sample and production flow-rate was equal to injection flow-rate).
4. Then, the injection of the vapour-saturated $scCO_2$ began at constant flow-rate (primary drainage flood). The displacement continued until steady-state conditions were reached. At the conclusion of this drainage process there was a so called "bump flow" (i.e. a short period of high injection flow-rate) performed to examine and quantify the existence of any capillary end-effect (Rapoport and Leas, 1953; Heaviside and Black, 1983; Grigg and Svec, 2006).
5. After the conclusion of the primary drainage, the core-sample was subjected to the primary imbibition flood. CO_2-saturated brine was injected into the sample at constant flow-rate. The brine injection continued until the steady-state conditions were achieved.
6. In the next step, for two of the experiments, the sample underwent another cycle of drainage-imbibition floods (secondary drainage and imbibition). For this purpose, steps number 5 and 6 were repeated again.
7. At the conclusion of the experiment, the core-holder was depressurised and the core sample was removed.

It is worth noting that during the procedure outlined above all the injected fluids passed through a 0.5 micron sintered stainless steel line filter before entering the core samples. This was to prevent any external fines being pushed into the pore space of the samples and potentially block and/or bridge the samples' pore channels.

4 Results

4.1 General characterization

Quantitative mineralogy by X-Ray Diffraction (XRD) indicates quartz and K-feldspar as the main constituents of these sandstones, with accessory kaolinite (up to 7% in sample 206660) (Table 2). Furthermore, sample 206660 contained 4% of ankerite, a calcium, iron, magnesium, manganese carbonate.

Table 2 summarizes the petrophysical properties of the pre-flood core-plugs, i.e. mercury porosity, helium porosities and permeabilities measured at the lowest effective stress (1.72 MPa) and brine permeability as well as mineralogy as measured by XRD. All the core-plugs displayed comparable values of porosity but a wider range of helium permeability (from 25 to 532 mD) and brine permeability (from 4.65 to 238 mD); also there is a good agreement between porosity measured by mercury injection on small offcuts (Figure 2c) and the values retried via He-porosimetry on the full core plugs. On the other hand, there is a significant difference between the values of He and water permeability. This is due the well-known Klinkenberg effect which is well described in the literature (Tiab and Donaldson, 2004).

Following the definition outlined by Sing et al. (1984), pore sizes can be classified as follows:

- Micropores: with widths smaller than 2 nm.
- Mesopores: with widths between 2 and 50 nm.
- Macropores: with widths larger than 50 nm.

MICP results show similar pattern for the three analysed samples (Figure 2b) with a narrow population of mesopores (cumulatively 2.5 to 3.5 % of the pore volume) while the rest of the pore sizes fall in the macropores range (> 50 nm); micropores could not be detected in the analysed samples. Samples 206647 and 206669 have a dominant pore population with throat diameter of ≈ 40 μm, while sample 206660 has a broad distribution of pores and the largest detected throat size of ≈ 30 μm which can explain its lower permeability with respect to the other samples.

4.2 Core flood tests

As indicated earlier, samples 206647 and 206669 underwent successive primary and secondary drainage and imbibition floods but samples 206655 and 206660 were tested for primary drainage and imbibition floods only. For all four samples, the end-point residual saturations obtained at the end of the drainage and imbibition floods are presented in Table 3 along with the corresponding end-point relative permeabilities for the displacing fluids.

Figure 4 shows the brine productions versus pore volumes of $scCO_2$ injected through the samples for the primary drainage floods conducted on all four samples. As may be expected, there is considerable volume of brine produced after $scCO_2$ breakthrough in the case of sample 206647. This may be attributed mainly to the high permeability of this sample leading to a more non-uniform or dispersed displacement (Saeedi et al., 2011; Saeedi, 2012) compared to other samples whose post breakthrough brine production profiles are comparable. The relative permeability curves corresponding to the above mentioned brine production profiles for three of the samples are also shown in Figure 5. While the end-point $scCO_2$ relative permeabilities for all samples are comparable, the curvature of the plots changes according to the samples permeabilities (i.e. the higher the permeability the higher the curvature). It is worth noting that the relative permeability data provided here were calculated using a numerical history matching technique (Archer and Wong, 1973; Sigmund and McCaffery, 1979; Bennion and Bachu, 2005). Sendra software from PRORES AS, which is based upon a two-phase, 1D black-oil simulation model together with an automated history matching routine, was used to reconcile time and spatially dependent experimental data and generate the relative permeabilities. This technique has three primary advantages over other relative permeability derivation techniques such as the JBN (Johnson, Bossler, and Naumann): 1. The relative permeability data can be derived directly for the full range of mobile $scCO_2$ and brine saturations and there is no need for extrapolation of this data as commonly done in other techniques such as the JBN, 2. Unlike other techniques such as the JBN where the effect of capillary pressure is ignored, the technique used here takes into account the effect of capillary pressure data. If such data is not available, a suitable model can be chosen to be used during the modelling and history matching procedure, 3. The output relative permeability data are automatically matched using one of the most commonly used relative permeability correlations (e.g. Corey, Sigmund and McCaffery, LET, etc.). This facilitates the integration of the derived relative permeability data into a full field numerical simulation model.

After performing the history matching routine for relative permeability calculation, the model proposed by Sigmund and McCaferry (1979) (Equations 1 to 3) was found to closely reproduce the measured data. This model was initially developed for interpretation of USS relative permeability measurements in heterogeneous cores where viscous–capillary effects are expected to be large and gravity effects are expected to be negligible. Thus, the Sigmund and McCaffery model is an ideal tool for interpreting the core–flood experiments performed here. Table 4 presents the values of the model parameters which resulted in the best match of the lab measured data by the Sigmund and McCaferry (1979) model.

$$k_{rw} = k_{rw}^{0} \frac{(S_w^*)^{N_w} + AS_w^*}{1 + A} \qquad \text{Eq. 1}$$

$$k_{rg} = k_{rg}^{0} \frac{(1 - S_w^*)^{N_g} + B(1 - S_w^*)}{1 + B} \qquad \text{Eq. 2}$$

$$S_w^* = \frac{S_w - S_{wi}}{1 - S_{wi} - S_{gi}} \qquad \text{Eq. 3}$$

where: k_{rw} and k_{rg} are the water and gas relative permeabilities at any saturation level.

k_{rw}^{0} and k_{rg}^{0} are the end-point (maximum) water and gas relative permeabilities.

S_w^* is the normalised water saturation as determined by Eq. 3.

S_{wi} and S_{gi} are the fixed residual water and gas saturations, respectively.

S_w is the variable water saturation measured during an USS experiment.

N_w, N_g, A and B are empirical constants used for the calculation of the relative permeabilities.

With regards to the experiments conducted in this work, in the above equations, subscript w would refer to the brine and subscript g would refer to $scCO_2$.

In an attempt to compare the results of the modelling work performed using Sendra with the output of another widely used numerical simulation software package, for Sample 206655, Eclipse simulation software (Schlumberger Inc.) was used to perform a core scale numerical simulation. For this task, after constructing a core scale grid model in Eclipse and populating the model with basic rock and fluid properties, the relative permeability data derived from Sendra were used as input data to simulate and generate the brine production and differential pressure profiles. Then a comparison was made between the experimental pressure and brine production data, which were fed into Sendra in the first place, and their simulated counterparts. As can be seen from figures 6 and 7, there is a very close agreement between the two sets of data. The rock and fluid properties used in the core scale model created using Eclipse are provided in Table 5.

Helium porosity and permeability as well as NMR porosity (and computed permeability) measured before and after core flooding experiments are summarized in Table 6. While porosity, measured by Helium and NMR, does not seem to be affected by the flooding procedure, permeability values significantly differ when measured on the same sample before and after flooding. Indeed, for sample 206647, the helium permeability measurement conducted on the post-flood dry sample showed a reduction of almost 25% compared to that of the pre-flood conditions. Samples 206655, 206660 and 206669 also showed permeability reductions of 60%, 51% and 44%, respectively. Using a classical T_2 surface relaxivity in sandstones from literature of about 20 µm/s (Marschall et al, 1995; Liu et al., 2014), the relaxation time T_2 distribution can be transformed into pore diameter distribution (Figure 8) assuming sphere-model for the pore network topology (Dunn et al., 2002; Sorland et al., 2007) as:

$$\frac{1}{T_2} = \rho\frac{S}{V} \cong \rho\frac{3}{r} \qquad \text{Eq. 4}$$

where S and V represent the surface and volume of the pore network, ρ is the surface relaxivity and r is the pore radius. Therefore, the equation 4 can be re-arranged as:

$$d_{NMR} = 6T_2\rho_{T2} \quad \text{Eq. 5}$$

where d_{NMR} is the pore body diameter (in μm) and ρ_{T2} is the surface relaxivity of about 20 μm/s for sandstones.

The converted NMR pore size distribution from the T_2 spectra using the equation 5 collected on samples 206647 and 206660 are shown in Figure 8 before and after flooding. The NMR pore size distribution and MICP pore throat size distribution (Figure 2a) give the same range of pore size on the pre-flooded samples with most of the pore size (or pore throat size) between 10 and 100 μm for 206647 and between 1 and 10 μm in 206660. The integrated NMR T_2 spectra curves give porosity values of about 14 and 15 % for samples 206647 and 206660, respectively, very similar to MICP and helium porosity data; remarkably the distributions collected in the samples after flooding show significant difference with respect to those collected before flooding. Specifically, it is observed that in both samples the curves are shifted towards shorter T_2 relaxation times; assuming a similar surface relaxivity (i.e. similar mineralogy and surface texture of the mineral in the pre- and post-flood samples), changes in the NMR T_2 relaxation time distribution in post-flood samples reflect alteration to the pore size distribution in the samples. In both samples, the larger pores observed at the right end of the spectrum seem to have disappeared after the flooding tests (> 80 μm in 206647 and > 4 μm in 206660) in favour of a higher relative proportion of medium size pores occurring at $T_2 = 2 \times 10^5$ and 10^4 ms for sample 206647 and 206660, respectively; which correspond after conversion into pore diameter at 30 μm in 206647 and 1.5 μm in 206660 (Figure 8).

5 Discussion

5.1 Residual trapping potential of the Lesueur Sandstone

The experimental results presented above provide the first assessment of multi-phase fluid flow behaviour in the potential reservoir of the South West Hub project, onshore Western Australia. As such, the relative permeability functions and measured end-point residual saturations can be used to populate large scale reservoir models to predict CO_2 injectivity and plume mobility over time. It is worth noting that the flood characteristics of the fluid-rock system (e.g. relative permeabilities) change continuously during the CO_2-brine flooding performed in the laboratory. Such changes are induced by the fluid-rock interactions which occur during such experiments. According to the Darcy's Law, with the occurrence of such reactions, the concept of relative permeability (which is based on and calculated using the Darcy's Law) may lose its meaning. Therefore, the application of the data reported in this study and perhaps other similar studies, is subject to the inherent uncertainties introduced due to the above mentioned reactions and transient effects.

In discussing the results of the core flooding tests, the maximum CO_2 saturation achieved during the drainage and the trapped saturation after the imbibition floods are referred to as S_{max} and S_t, respectively, following the nomenclature commonly used in the literature (e.g. Burnside and Naylor, 2014) and use the ratio of S_t to S_{max} (i.e. R) to assess the fraction of CO_2 immobilised in the pore space of a sample. These parameters are useful to quantify the residual trapping potential of the Lesueur Sandstone and help predict its impact on the CO_2 storage security at the reservoir scale.

Figure 9 illustrate the relationship between S_{max} and S_t obtained on the four samples of Lesueur Sandstone tested in this study in comparison with experimental data obtained on sandstone samples from different studies available in the open literature (Bennion and Bachu, 2008; ; Mackay et al., 2010; Pentland et al., 2011a, b; Shell, 2011; Shi et al., 2011a, b; Krevor et al., 2012; Bachu, 2013). Laboratory derived values available for sandstone reservoirs show S_{max} ranging between 0.31 and 0.85 and S_t between 0.1 and 0.52; the Lesueur Sandstone samples tested in this study show a relatively narrow range of S_{max} ($0.55 < S_{max} < 0.61$), while residual CO_2 saturation is more variable ($0.23 < S_t < 0.44$). Finally, the percentage of the residually trapped CO_2 with reference to S_{max} (i.e. $R = \frac{S_t}{S_{max}}$) ranges between 41.58 and 73.20 % for the Lesueur Sandstone samples (Table 7) with an average value of 61.02 %, in good agreement with the mean sandstone value of 61 % reported by Burnside and Naylor (2014).

The relationship between the maximum and residual saturations of the non-wetting fluid is often estimated using the empirical trapping model developed by Land (1968) to predict the trapped gas saturation as a function of the initial gas saturation. According to the model, residual saturation can be calculated as:

$$S_t = \frac{S_{max}}{1 + CS_{max}} \qquad \text{Eq. 6}$$

Where C is the trapping coefficient calculated as:

$$C = \frac{1}{S_t} - \frac{1}{S_{max}} \qquad \text{Eq. 7}$$

It can be seen in Figure 9 that experimental observations of residual trapping of supercritical CO_2 reported in sandstone reservoirs are generally bounded by the Land's trapping coefficient range of 0.2 < C < 5 and that the Lesueur Sandstone samples exhibit a range of C between 0.63 and 2.55 (Table 7).

5.2 Fluid-rock interaction and resulting permeability degradation

The characterization analysis conducted on the samples before and after core flooding tests indicate a significant alteration of some of their petrophysical properties. While the overall porosity remains almost unchanged, the most evident modifications are seen in a systematic reduction of permeability (measured by He permeametry) observed on the four samples analysed after flooding (Figure 10 and Table 6) and in the NMR T_2 spectra collected on the brine saturated samples showing shorter T_2 (i.e. less movable water) (Figure 8). The observed variations could be attributed to the fluid-rock interactions occurred during the flooding experiments.

Fluid rock interactions during flooding of siliciclastic reservoirs with supercritical CO_2 and CO_2-saturated brines can be observed in nature (e.g. Bowker et al., 1991; Emberly et al., 2005; Assayag et al., 2009) and in laboratory experiments (e.g. Berrezueta et al., 2013; Huq et al., 2014; Pudlo et al., 2015) with consequences reported on the permeability (Sayegh et al., 1990; Pudlo et al., 2015; Yasahura et al., 2015) and elastic/mechanical properties of the host rock (Daley et al., 2007; Oikawa et al., 2008; Zheng et al., 2015; Delle Piane and Sarout, submitted).

Injection of carbon dioxide into a brine saturated reservoir will result in the formation of carbonic acid which, in turn, will likely react with the minerals constituting the porous frame of the rock, inducing mineral dissolution and/or precipitation. Common reactions within quartz rich sandstone reservoirs include the dissolution of carbonate and evaporite cements and the dissolution of alkali feldspar and clay minerals (e.g. Gaus, 2010 and references therein). Mineral dissolution would result in an increase in porosity which was not observed in our samples indicating that this fluid-rock interaction mechanism was not dominant at the experimental conditions explored in this study.

Alternative mechanisms that could explain the observed decrease in permeability and shift in NMR spectra are mineral precipitation and particle migration within the pore space of the rocks. Based on the mineralogy of the Lesueur samples, potential reactive phases identified in all tested samples are K-feldspar and kaolinite, while the only sample with quantifiable carbonate material was 206660 (see Table 2). While feldspar reaction rates are rather sluggish at the experimental conditions explored in this study, clay minerals and carbonates can react with carbonic acid quite rapidly, which can lead to pore space geometry changes in a relatively short time (e.g. Vialle and Vanorio, 2011; Pudlo et al., 2015). Clay minerals, in particular, are very susceptible to changes in the surface layer chemistry, and recent experimental studies pointed out that CO_2 can be adsorbed onto kaolinite (Schaef et al. 2014) and that interactions between clay minerals and supercritical CO_2 and acidified brines can lead to detachment and partial removal of inter-granular clay from the rock matrix as a consequence of CO_2 diffusion within the clay layer structures and related changes in the interlayer electrical forces (Berrezueta et al., 2013; Wilson et al., 2014).

Kaolinite is the one of the clay minerals identified in the Lesueur Sandstone (Olierook et al., 2014) and is detected by XRD in the samples used for core flooding (Table 2); it occurs as an authigenic phase showing different habits including fine grained, pore occluding (Figure 11a) and pore bridging (Figure 11b) aggregates; booklets and vermicules growing on quartz grain surfaces (Figure 11c) and euhedral, well crystallized and coarse grained (Figure 11d). It is evident that even within the same sample, kaolinite crystals display considerable variation in terms of morphology and size and therefore specific surface area, a critical parameter dictating the capacity of interactions with pore fluids.

Alteration of brine salinity and pH has been shown to modify the electrical charge of kaolinite and cause repulsive forces leading to dispersion from its aggregate form and mobilization within the pore space, i.e. fines migration (Lemon et al., 2011; Wilson et al., 2014), which in turn can negatively affect permeability in sandstone as previously reported for example by Bennion et al. (1992), Kummerow and Spangenberg (2011), Sell et al. (2013) and Pudlo et al. (2015)

The role of fines migration in the permeability reduction of the post-flood samples is further reaffirmed by the fact that while permeability values of the samples were reduced after undergoing the flooding procedure, the changes in their porosity values were not appreciable. This is in line with what has been reported in the literature by other researchers (Morris and Shepperd, 1982; Priisholm et al., 1987; Hayatdavoudi and Ghalambor, 1996; Musharova et al., 2012). In fact, existence of kaolinite particles in the pore space of sample 206669 is evident from the Scanning Electron Microscopy (SEM) images taken from the offcuts of this sample (Figure 11). During the flooding process, these particles could dislodge and while moving towards the samples downstream could plug and/or bridge the samples pore throats.

6 Summary and Conclusions

Four conventional USS core-flooding experiments were conducted on different core-plugs from the Wonnerup Member of the Lesueur Formation. The main data generated by the experiments included residual $scCO_2$ and brine saturations and relative permeabilities for the drainage and imbibition floods. Overall, the experimental results indicate that significant quantities of CO_2 were trapped in the Lesueur Sandstone samples by capillary forces, as a result of imbibition under in-situ reservoir conditions. While the residual $scCO_2$ saturations obtained were relatively high, they are inversely proportional to the samples' absolute permeabilities, as one may expect. Initial and residual saturations measured in this study seem consistent with values published in the literature from sandstones reservoir samples.

Once flooded, the samples showed about 25%-60% reduction in permeability while the changes in their porosity values were almost negligible. The results of all the auxiliary analysis performed point towards fines migration to be the likely cause of the permeability reductions observed. This phenomenon can have a significant and detrimental effect on CO_2 injectivity, and most likely can affect the near wellbore region where fluid flow and chemical/physical alteration of the formation brine are maximised.

Given the petrological and petrophysical nature of the Lesueur Sandstone, it is believed that the results presented here could be relevant for other sandstone reservoirs with similar mineralogy, being considered for CO_2 geo-sequestration. A better understanding of the influence of isolated variables (e.g. fluid pH or salinity) on the magnitude of permeability reduction should be the focus of future research.

7 Acknowledgements

The authors wish to acknowledge financial assistance provided through Australian National Low Emissions Coal Research and Development (ANLEC R&D). ANLEC R&D is supported by Australian Coal Association Low Emissions Technology Limited and the Australian Government through the Clean Energy Initiative. This manuscript has been prepared based on the data and information generated in ANLEC R&D funded project 7-1111-0199.

The authors would also like to acknowledge Geotech Geotechnical Services PTY LTD for their help during the sample characterisation stage of this work. We also would like to acknowledge the help from PRORES AS for granting us the access to their core-flood interpretation software package, Sendra.

8 References

Akbarabadi, M., Piri, M., 2013. Relative permeability hysteresis and permanent capillary trapping characteristics of supercriticalCO_2/brine systems: an experimental study at reservoir conditions. Advances in Water Resources. 52, 190–206.

Archer, J. S., and S. W. Wong, 1973, Use of a reservoir simulator to interpret laboratory waterflood data: SPE 3551, SPE Journal, v. 13, p. 343-347.

Assayag, N., J. Matter, M. Ader, D. Goldberg, and P. Agrinier., 2009. Water–rock interactions during a CO_2 injection field-test: implications on host rock dissolution and alteration effects. *Chemical Geology* 265, no. 1 : 227-235.

Bachu, S., 2012. Drainage and imbibition of CO_2/brine relative permeability curves at in situ conditions for sandstone formations in western Canada. Proceedings of the 11th International Conference on Greenhouse Gas Control Technologies, November 18–22, Kyoto, Japan, Elsevier, Energy Procedia, v. 37 (2013), pp. 4428–4436

Baker, R.W. and Low, B.T., 2014. Gas Separation Membrane Materials: A Perspective. Macromolecules, 47(20): 6999-7013.

Bear, J., 1988. Dynamics of Fluids in Porous Media. Dover Publications Inc., New York

Bennion, D.B. and Bachu, S., 2008. Drainage and imbibition relative permeability relationships for supercritical CO2/brine and H2S/brine systems in intergranular sandstone, carbonate, shale, and anhydrite rocks. SPE Reservoir Evaluation and Engineering, 11, pp. 487–496

Bennion, B. and Bachu, S., 2005. Relative permeability characteristics for supercritical CO_2 displacing water in a veriety of potential sequestration zones in the Western Canada sedimentary basin, SPE 95547, The SPE annual technical conference and exhibition. Society of Petroleum Engineers, Dallas, Texas, USA.

Bennion, D.B., Thomas, F.B., Bennion, D.W. and Bietz, R.F., 1995. Mechanisms of formation damage and permeability impairement associated with the drilling, completion and production of low API gravity oil reservoirs. SPE 30320.

Bennion, D.B., Bietz, R.F., Thomas, F.B. and Cimolai, M.,1994. Reductions in the Productivity of Oil and Low Permeability Gas Reservoirs Due to Aqueous Phase Trapping. Journal of Canadian Petroleum Technology 33, No. 9

Bennion, D.B., Scott, JA. and Bennion, D.W., 1992. Detailed Laboratory Studies of Chemically and Biologically Induced Formation Damage in the East Wilmington Field, paper CIM 92-44 presented at the ATM of the Petroleum Society of CIM (May 7-10, 1992).

Berrezueta, E., L. González-Menéndez, D. Breitner, and L. Luquot., 2013. Pore System Changes during Experimental CO2 Injection into Detritic Rocks: Studies of Potential Storage Rocks from Some Sedimentary Basins of Spain, International Journal of Greenhouse Gas Control 17. Elsevier Ltd: 411–22. doi:10.1016/j.ijggc.2013.05.023.

Bowker, Kent A., and P. J. Shuler.,1991. Carbon dioxide injection and resultant alteration of the Weber Sandstone, Rangely Field, Colorado (1). *AAPG Bulletin* 75, No. 9 : 1489-1499.

Burnside, N. M., and M. Naylor., 2014. Review and implications of relative permeability of CO_2/brine systems and residual trapping of CO_2. International Journal of Greenhouse Gas Control 23 : 1-11.

Busch, A., Alles, S., Gensterblum, Y., Prinz, D., Dewhurst, D.N., Raven, M.D., Stanjek, H., Krooss, B.M., 2008. Carbon dioxide storage potential of shales. International Journal of Greenhouse Gas Control 2, 297–308

Cheneviere, P., Sardin, M., de Farcy, P. and Putz, A., 1992. An equilibrium model for describing the transient transport of particles in porous media. Phys. Chem. Colloids Interfaces Oil Production. H. Toulhoat, J. Lecourtier (eds.) and editions Technip, 317-332.

Daley, Thomas M., Larry R. Myer, J. E. Peterson, E. L. Majer, and G. M. Hoversten. 2007. “Time-Lapse Crosswell Seismic and VSP Monitoring of Injected CO_2 in a Brine Aquifer.” Environmental Geology 54 (8): 1657–65. doi:10.1007/s00254-007-0943-z.

Delle Piane, C., Esteban, L., Timms, N.E. and Ramesh Israni, S., 2013a. Physical properties of Mesozoic sedimentary rocks from the Perth Basin, Western Australia. Australian Journal of Earth Sciences, 60(6-7): 735-745.

Delle Piane, C., Olierook, H.K.H., Timms, N.E., Saeedi, A., Esteban, L., Rezaee, R., Mikhaltsevitch, V., Lebedev, Maxim. 2013b. Facies-based rock properties distribution along the Harvey 1 stratigraphic well. CSIRO Report Number EP133710. ANLEC Project Projects 7-1111-0199: http://www.anlecrd.com.au/_literature_146941/Facies-based_rock_properties_distribution_along_the_Harvey-1_stratigrap

Delle Piane, C. and Sarout J. Effects of water and supercritical CO_2 on the mechanical and elastic properties of Berea sandstone. Submitted to International Journal of Greenhouse Gas Control.

DeVore, G.W., 1957. The surface chemistry of feldspars as an influence on their decomposition products. Clays and clay minerals, vol. 6, 1, 26-41.

Dillinger, A. and Esteban, L., 2014. Experimental evaluation of reservoir quality in Mesozoic formations of the Perth Basin (Western Australia) by using a laboratory low field Nuclear Magnetic Resonance. Marine and Petroleum Geology, 57(0): 455-469.

Doughty, C., & Pruess, K. (2004). Modeling supercritical carbon dioxide injection in heterogeneous porous media. Vadose Zone Journal, *3*(3), 837-847.

Dullien, F.A.L.: Porous Media: Fluid Transport and Pore Structure. Academic Press Inc., New York (1992)

Dunn, K.J., Bergman, D.J. and LaTorraca, G.A., 2002. Nuclear magnetic resonance: Petrophysical and logging applications. Elsevier.

Emberley, S., I. Hutcheon, M. Shevalier, K. Durocher, B. Mayer, W. D. Gunter, and E. H. Perkins. Monitoring of fluid–rock interaction and CO_2 storage through produced fluid sampling at the Weyburn CO_2 injection enhanced oil recovery site, Saskatchewan, Canada. Applied Geochemistry 20, no. 6 (2005): 1131-1157.

Gaus, Irina. Role and impact of CO_2–rock interactions during CO_2 storage in sedimentary rocks. *International journal of greenhouse gas control* 4, no. 1 (2010): 73-89.

Garrels, R.M. and Howard, P., 1959. Reactions of feldspar and mica with water at low temperature and pressure. Geochem. Cosmochim. Acta, 50, 1847-1860.

Grigg, R.B. and Svec, R.K., 2006. CO_2 transport mechanisms in CO_2/brine core flooding, SPE 103228, SPE Annual Technical Conference and Exhibition. Society of Petroleum Engineers, San Antonio, Texas, USA.

Hayatdavoudi, A. and Ghalambor, A., 1996. Controlling Formation Damage Caused by Kaolinite Clay Minerals: Part I, SPE Formation Damage Control Symposium. Copyright 1996, Society of Petroleum Engineers Inc., Lafayette, Louisiana.

Heaviside, J. and Black, C.J.J., 1983. Fundamentals of relative permeability: experimental and theoretical considerations, SPE 12173, SPE Annual Technical Conference and Exhibition. Society of Petroleum Engineers of AIME, San Francisco, California.

Huq, Farhana, Stefan B. Haderlein, Christian Schröder, Michael AW Marks, and Peter Grathwohl. Effect of injected CO_2 on geochemical alteration of the Altmark gas reservoir in Germany. Environmental Earth Sciences 72, no. 9 (2014): 3655-3662.

IPCC: IPCC Special Report on Carbon dioxide Capture and Storage—Summary for Policymakers, Report, Intergovernmental Panel on Climate Change, Montreal, Canada, 25 pp (2005).

Izgec, O., Demiral, B., Bertin, H. and Akin, S., 2008. CO_2 injection into saline carbonate aquifer formations I: laboratory investigation Transport in porous media, 72(1): 1-24.

Jorand, R., Fehr, A., Koch, A. and Clauser, C., 2011. Study of the variation of thermal conductivity with water saturation using nuclear magnetic resonance. Journal of Geophysical Research: Solid Earth, 116(B8): B08208.

Khan, L. and Hasan, M., 2007. Enhancement of hydrophyllic characteristics of non-wetting porous substrates by kaolinite treatment. SAE technical paper, 2007-01-3178, doi: 10.4271/2007-01-3178.

Kleinberg, R.L. et al., 2003a. Deep sea NMR: Methane hydrate growth habit in porous media and its relationship to hydraulic permeability, deposit accumulation, and submarine slope stability. Journal of Geophysical Research: Solid Earth, 108(B10): 2508.

Kleinberg, R.L. et al., 2003b. Seafloor nuclear magnetic resonance assay of methane hydrate in sediment and rock. Journal of Geophysical Research: Solid Earth, 108(B3): 2137.

Kopp, A., H. Class, and R. Helmig (2009), Investigations on CO_2 storage capacity in saline aquifers Part 1. Dimensional analysis of flow processes and reservoir characteristics, Int. J. Greenhouse Gas Control, 3, 263–276

Krevor, S.C.M., Pini, R., Zuo, L., Benson, S.M. Relative permeability and trapping of CO_2 and water in sandstone rocks at reservoir conditions. Water Resource Research, 48 (2012), p. W02532 http://dx.doi.org/10.1029/2011WR010859

Kummerow, Juliane, and Erik Spangenberg. Experimental evaluation of the impact of the interactions of CO_2-SO_2, brine, and reservoir rock on petrophysical properties: A case study from the Ketzin test site, Germany. *Geochemistry, Geophysics, Geosystems* 12, no. 5 (2011).

Labus, K., 2010. Modeling CO_2 sequestration mechanisms, and capacity of carboniferous aquifer rocks of the Upper Silesian Coal Basin (Poland, Czech Republic). Water-rock interaction - Birkle & Torres-Alvarado (eds.), Taylor & Francis Group, London, ISBN: 978-0-415-60426-0, 871-875.

Land CS (1968) Calculation of imbibition relative permeability for two and three-phase flow from rock properties. Society of Petroleum Engineers Journal, 8, 149–56.

Lemon, Phillip Edward, Abbas Zeinijahromi, Pavel G. Bedrikovetsky, and Ibrahim Shahin. Effects of injected water chemistry on waterflood sweep efficiency via induced fines migration. In *SPE* International Symposium on Oilfield Chemistry. Society of Petroleum Engineers, 2011.

Li, X., Akbarabadi, M., Karpyn, Z.T., Piri, M., Bazilevskaya, E., 2015. Experimental investigation of carbon dioxide trapping due to capillary retention in saline aquifers. Geofluids, http://dx.doi.org/10.1111/gfl.12127.

Liu, H., D'Eurydice, M.N.m Obruchkiv, S. and Galvosas, P., 2014. Pore length scales and pore surface relaxivity of sandstone determined by internal magnetic fields modulation at 2 MHz NMR. Diffusion fundamentals, 22, 7, 1-5.

Lu, J., Kordi, M., Hovorka, S.D., Meckel, T.A., Christopher, C.A., 2012. Reservoir characterisation and complications for trapping mechanisms at Cranfield CO_2 injection site. Int. J. Greenh. Gas Control.

Mackay, E., Pickup, G., Olden, P. Rock mechanics, geochemistry and aquifer fluid flow. CASSEM Conference, 4th October 2010, Edinburgh (2010)

Manrique, E.J., Muci, V.E., Gurfinkel, M.E.: EOR field experiences in carbonate reservoirs in the United States. SPE Reserv. Eval. Eng. 10, 667–686 (2007)

Millar, AS and Reeve, J (compilers) 2014, GSWA Harvey 1 well completion and preliminary interpretation report, southern Perth Basin:Geological Survey of Western Australia, Record 2014/12, 17p.

Morris, K.A. and Shepperd, C.M., 1982. The role of clay minerals in influencing porosity and permeability characteristics in the bridport sands of wytch farm, dorset. Clay Minerals, 17: 41-54.

Morriss, C.E., Maclnnis, J., Freedman, R. and Smaardyk, J., 1993. Field Test Of An Experimental Pulsed Nuclear Magnetism Tool, SPWLA 34th Annual Logging Symposium. Society of Petrophysicists and Well-Log Analysts, Calgary, Alberta

Müller, N. (2011). Supercritical CO_2-brine relative permeability experiments in reservoir rocks—Literature review and recommendations. Transport in porous media, 87(2), 367-383.

Musharova, D., Mohamed, I.M. and Nasr-El-Din, H.A., 2012. Detrimental Effect of Temperature on Fines Migration in Sandstone Formations, SPE International Symposium and Exhibition on Formation Damage Control. Society of Petroleum Engineers, Lafayette, Louisiana, USA.

Nicot, B., Gautier, S., Fleury, M. and Durucan, S., 2006. Pore Structure Analysis of Coals Suing Low Field NMR Measurements and Thermogravimetric Analysis, SCA2006-27, The International Symposium of the Society of Core Analysts, Trondheim, Norway

Oikawa, Y., T. Takehara, and T. Tosha. Effect of CO_2 injection on mechanical properties of Berea Sandstone. In The 42nd US Rock Mechanics Symposium (USRMS). American Rock Mechanics Association, 2008.

Olierook, H.K.H. et al., 2014. Facies-based rock properties characterization for CO_2 sequestration: GSWA Harvey 1 well, Western Australia. Marine and Petroleum Geology, 50: 83-102.

Marschall, D., Gardner, J.S., Mardon, D. and Coates, G.R., 1995. Method for correlating NMR relaxometry and mercury injection data. SCA, Conference paper 9511, 1-12.

Pentland, C.H., El-Maghraby, R., Iglauer, S., Blunt, M.J., 2011. Measurements of the capillary trapping of super-critical carbon dioxide in Berea sandstone. Geophys. Res. Lett. 38, L06401.

Pentland, C.H., El-Maghraby, R. Georgiadis, A., Iglauer, S. Blunt, M.J. Immiscible displacements and capillary trapping in CO_2 storage. Energy Procedia, 4 (2011), pp. 4969–4976

Perrin, J.-C. and Benson, S.M., 2010. An experimental study on the influence of sub-core scale heterogeneities on CO_2 distribution in reservoir rocks. Transport in porous media, 82(1): 93-109.

Priisholm, S., Nielsen, B.L. and Haslund, O., 1987. Fines migration, blocking, and clay swelling of potential geothermal sandstone reservoirs, Denmark. SPE 15199, SPE Formation Evaluation, 2(2): 168-178.

Pudlo, Dieter, Steven Henkel, Viktor Reitenbach, Daniel Albrecht, Frieder Enzmann, Katja Heister, Geertje Pronk, Leonhard Ganzer, and Reinhard Gaupp. The chemical dissolution and physical migration of minerals induced during CO_2 laboratory experiments: their relevance for reservoir quality. Environmental Earth Sciences 73, no. 11 (2015): 7029-7042.

Rapoport, L.A. and Leas, W.J., 1953. Properties of linear waterfloods. SPE 213-G, Petroleum Transactions, AIME, 198: 139-148.

Ruprecht, C., Pini, R., Falta, R., Benson, S., Murdoch, L., 2014. Hysteretic trapping and relative permeability of CO_2 in sandstone at reservoir conditions. Int. J. Greenh. Gas Control 27, 15–27.

Saeedi, A., 2012. Experimental Study of Multiphase Flow in Porous Media during CO_2 Geo-Sequestration Processes. Sprinegr Thesis. Springer Publishing, Heidelberg, Germany.

Saeedi, A., Rezaee, R., Evans, B. and Clennell, B., 2011. Multiphase flow behaviour during CO_2 geo-sequestration: Emphasis on the effect of cyclic CO_2-brine flooding. Journal of Petroleum Science and Engineering, 79(3-4): 65-85.

Schaef, H T, V.-a. Glezakou, a T Owen, S Ramprasad, P F Martin, and B. P. McGrail. 2014. Surface Condensation of CO_2 onto Kaolinite. *Environmental Science & Technology Letters* 1 (2): 142–45. doi:10.1021/ez400169b

Sell, Kathleen, Frieder Enzmann, Michael Kersten, and Erik Spangenberg. Microtomographic quantification of hydraulic clay mineral displacement effects during a CO_2 Sequestration experiment with saline aquifer sandstone. *Environmental science & technology* 47, no. 1 (2012): 198-204.

Shell. UK Carbon Capture and Storage Demonstration Competition. UKCCS-KT-S7.19-Shell-002, SCAL Report ScottishPower CCS Consortium (2011), p. 59.

Shi, J-Q., Xue, Z., Durucan, S., 2011a. Supercritical CO2 core flooding and imbibition in Berea sandstone—CT imaging and numerical simulation Energy Procedia, 4 (2011), pp. 5001–5008

Shi, J-Q., Xue, Z., Durucan, S., 2011b. Supercritical CO_2 core flooding and imbibitions in Tako sandstone – influence of sub-core scale heterogeneity. Int. J. Greenh. Gas Control 5, 75–87

Sigmund, P.M. and McCaffery, F.G., 1979. An improved unsteady-state procedure for determining the relative-permeability characteristics of heterogeneous porous media. SPE 6720, SPE Journal, 19(1): 15-28.

Sing K, Everett D, Haul R, Moscou L, Pierotti R, Rouquérol J, Siemieniewska T (1985). IUPAC Commission on colloid and surface chemistry including catalysis. Reporting physisorption data for gas/solid systems with special reference to the determination of surface area and porosity (Recommendations 1984). Pure Appl Chem 57:603–619

Sorland, G.H., Djurhuus, K., Wideroe, H.C., Lien, J.R. and Skauge, A., 2007. Absolute pore size distributions from NMR. Diffusion fundamentals, 5, 4.1-4.15.

Suekane, T., Nobuso, T., Hirai, S., Kiyota, M., 2008. Geological storage of carbon dioxide by residual gas and solubility trapping. Int. J. Greenh. Gas Control 2, 58–64

Timms N.E., Olierook, H.K.H., Wilson, M.E.J., Delle Piane, C., Hamilton, P.J., Cope, P., Stutenbecker, L. 2015. Sedimentary facies analysis, mineralogy and diagenesis of the Mesozoic aquifers of the central Perth Basin. Marine and Petroleum Geology, 60, 54-78.

Vialle, Stéphanie, and Tiziana Vanorio. Laboratory measurements of elastic properties of carbonate rocks during injection of reactive CO_2-saturated water. *Geophysical Research Letters* 38, no. 1 (2011).

Wilson, M. J., L. Wilson, and I. Patey. The influence of individual clay minerals on formation damage of reservoir sandstones: a critical review with some new insights. *Clay Minerals* 49, no. 2 (2014): 147-164.

Yasuhara, Hideaki, Naoki Kinoshita, Hiroaki Ohfuji, Manabu Takahashi, Kazumasa Ito, and Kiyoshi Kishida. Long-term observation of permeability in sedimentary rocks under high-temperature and stress conditions and its interpretation mediated by microstructural investigations. *Water Resources Research* 51, no. 7 (2015): 5425-5449.

Zheng, Hong, Xia-Ting Feng, and Peng-Zhi Pan. Experimental investigation of sandstone properties under CO_2–NaCl solution-rock interactions. International Journal of Greenhouse Gas Control 37 (2015): 451-470.

Zuo, L., Benson, S.M., 2014. Process-dependent residual trapping of CO_2 in sandstone. Geophys. Res. Lett. 41, 2820–2826.

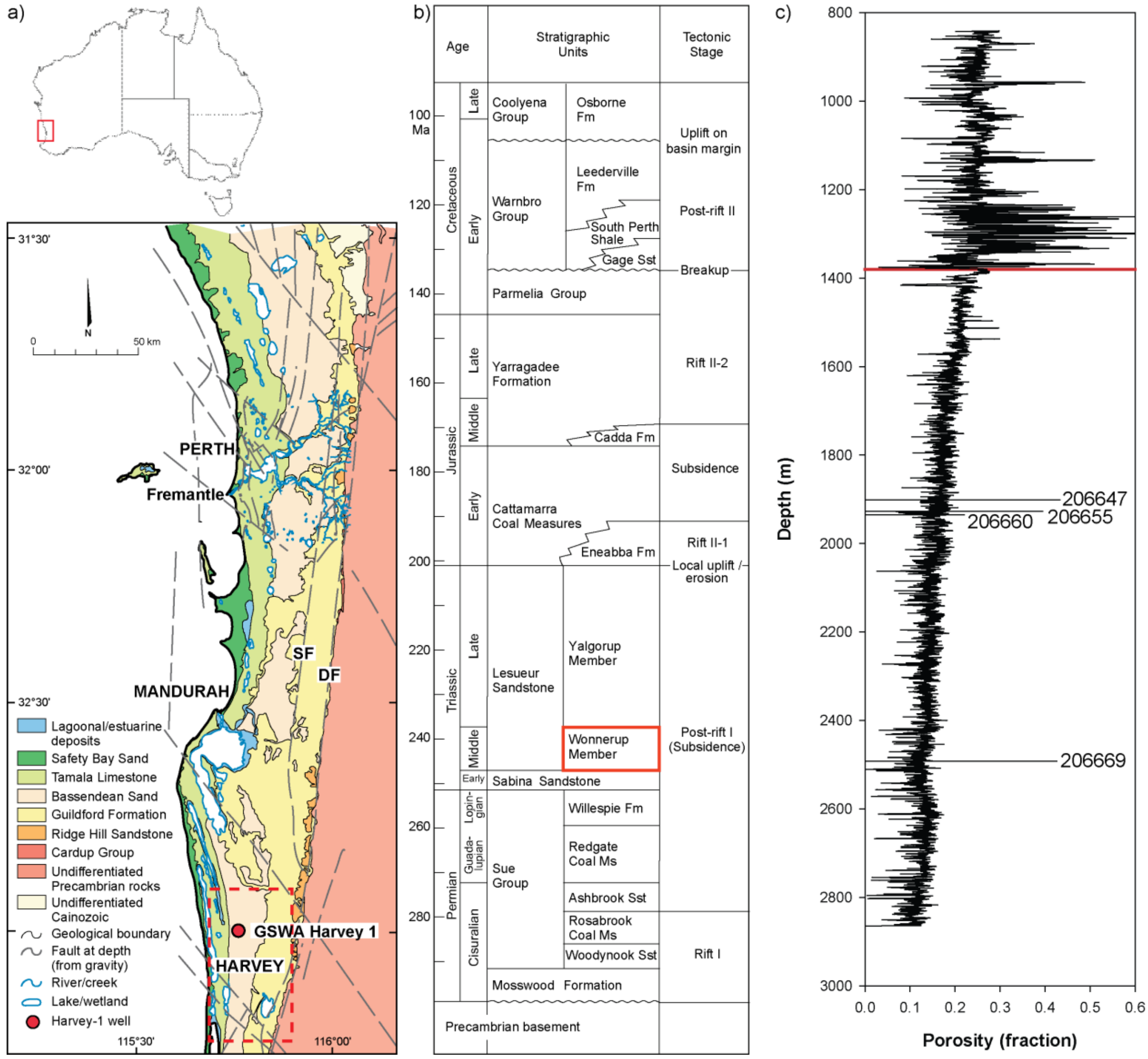

Figure 1 (a) Location of the Harvey-1 well and surface geology of the Perth Basin, the red dashed box indicates the approximate location of the proposed South-West Hub; (b) Stratigraphy of the Central and Southern Perth Basin, the studied section is highlighted in red (modified after Olierook et al., 2014); (c) wireline log of porosity along the Harvey 1 well: black horizontal lines indicate the depth of each sample used in this study; red horizontal lines marks the transition between the Wonnerup and the Yalgorup Members of the triassic Lesueur Sandstone

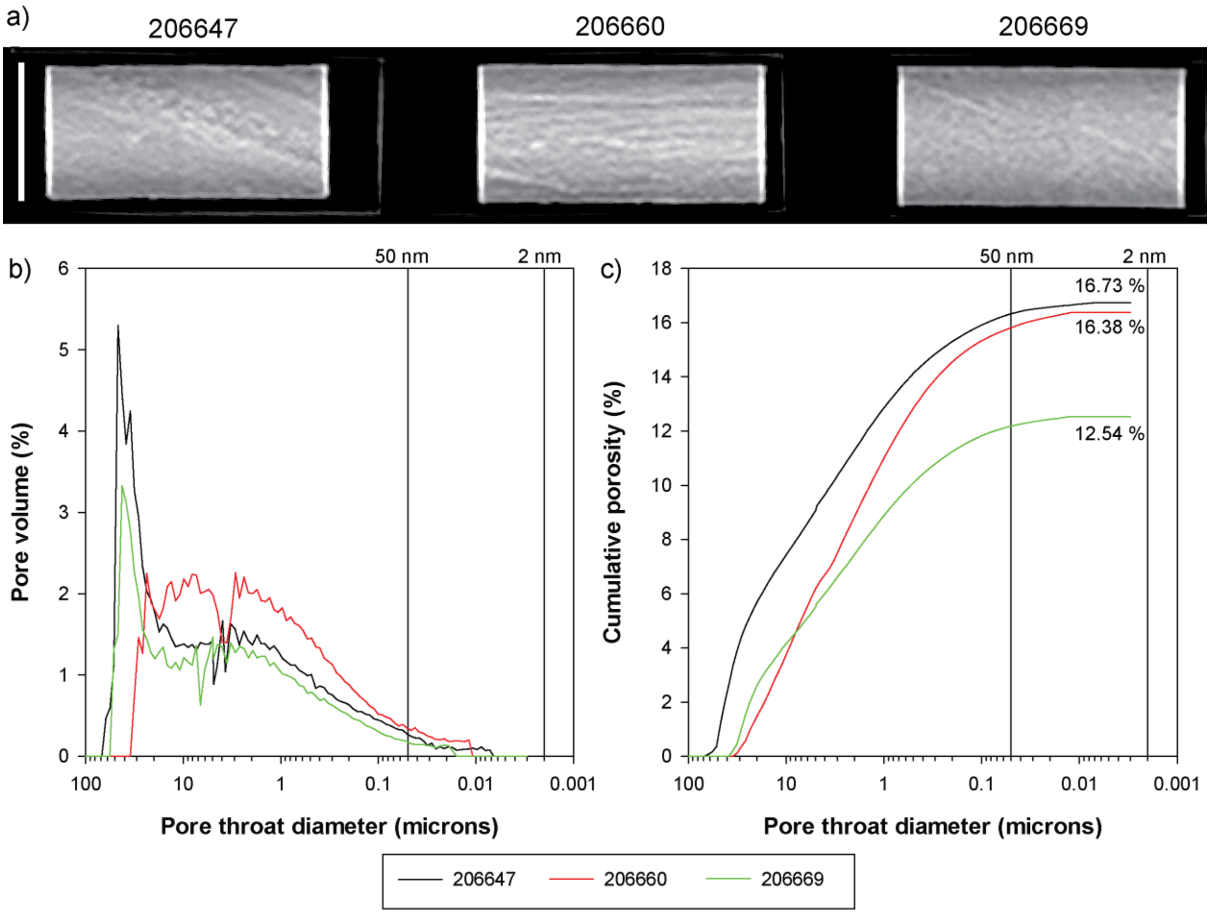

Figure 2 (a) X-ray CT images of three samples prior to core-flooding tests with their corresponding bulk density. (b) pore size distribution as measured by mercury injection porosimetry on offcuts of the three samples; vertical lines mark the boundaries between micropores (< 2 nm), mesopores (2-50 nm); and macropores (> 50 nm); (c) cumulative porosity as a function of pore throat size as measured by mercury injection.

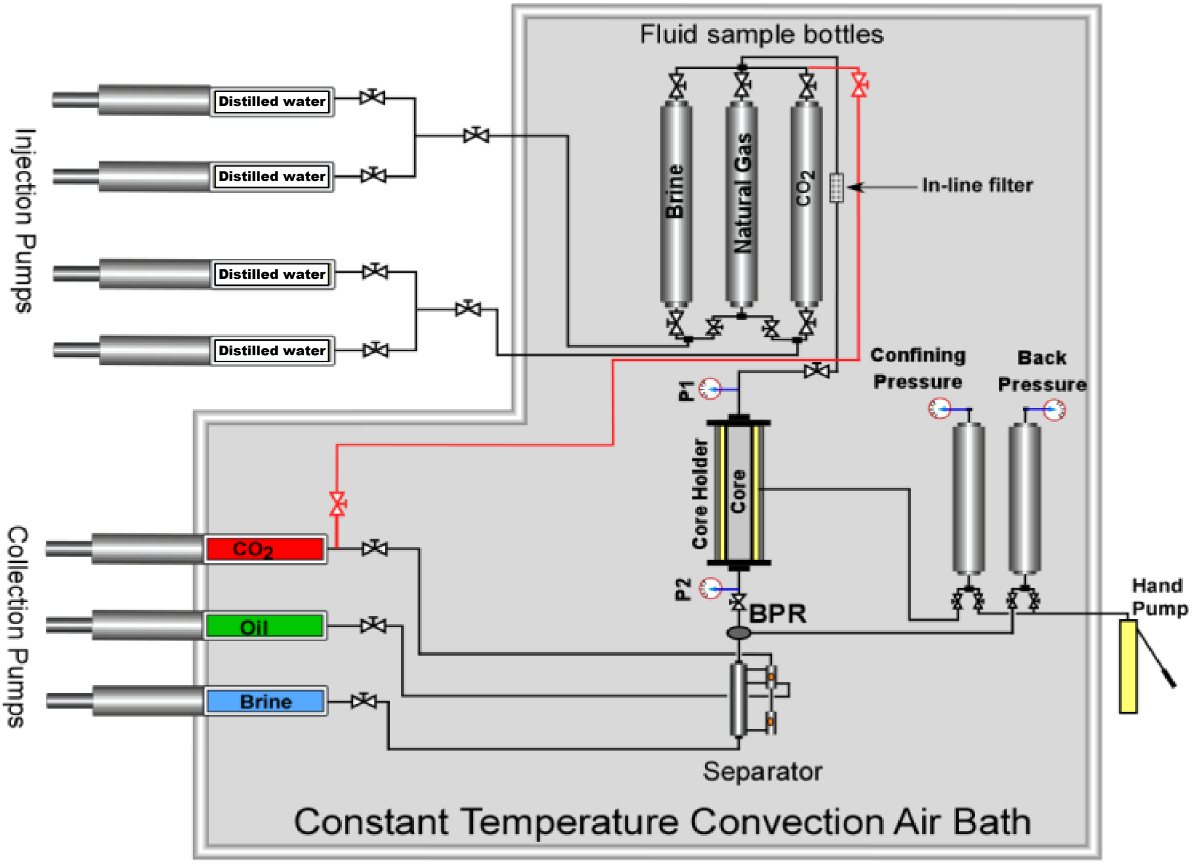

699
700 **Figure 3. The schematic diagram of the experimental apparatus used to run the core-flooding experiments.**

701

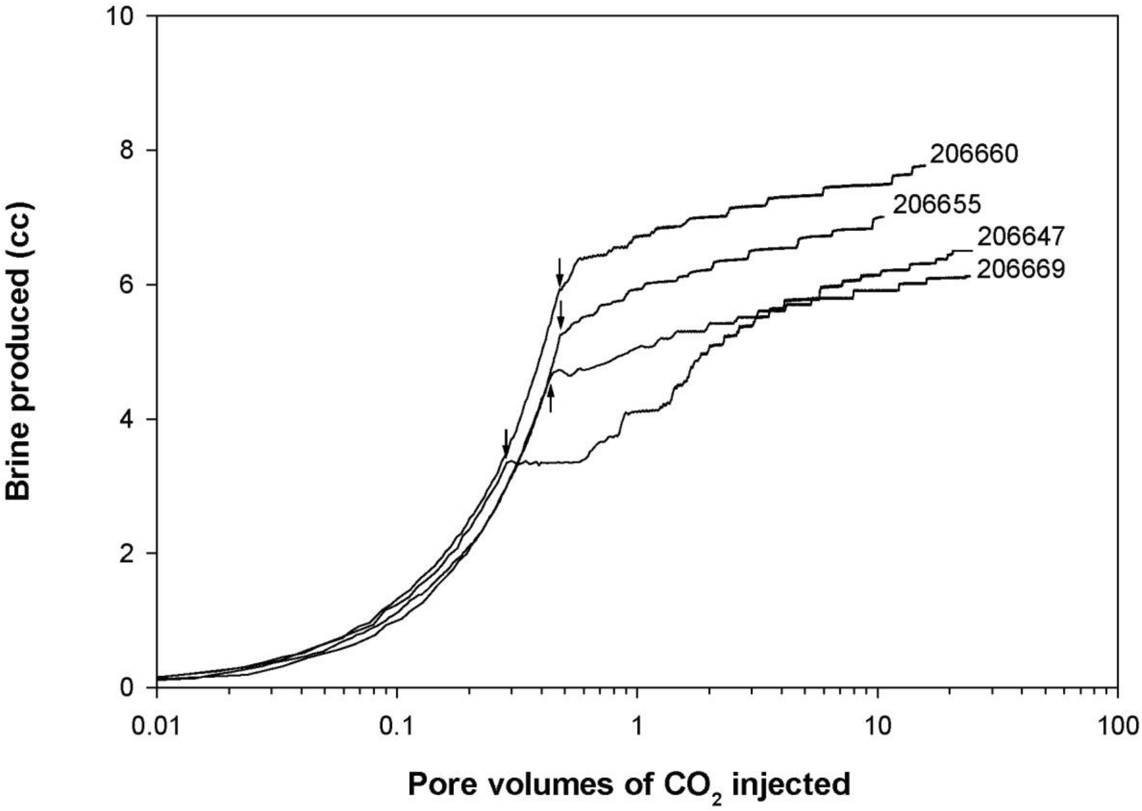

Figure 4. Brine production profiles for the primary drainage conducted on three out of the four samples; breakthrough of CO_2 is indicated by the black arrow and corresponds to the change in slope of the production curves.

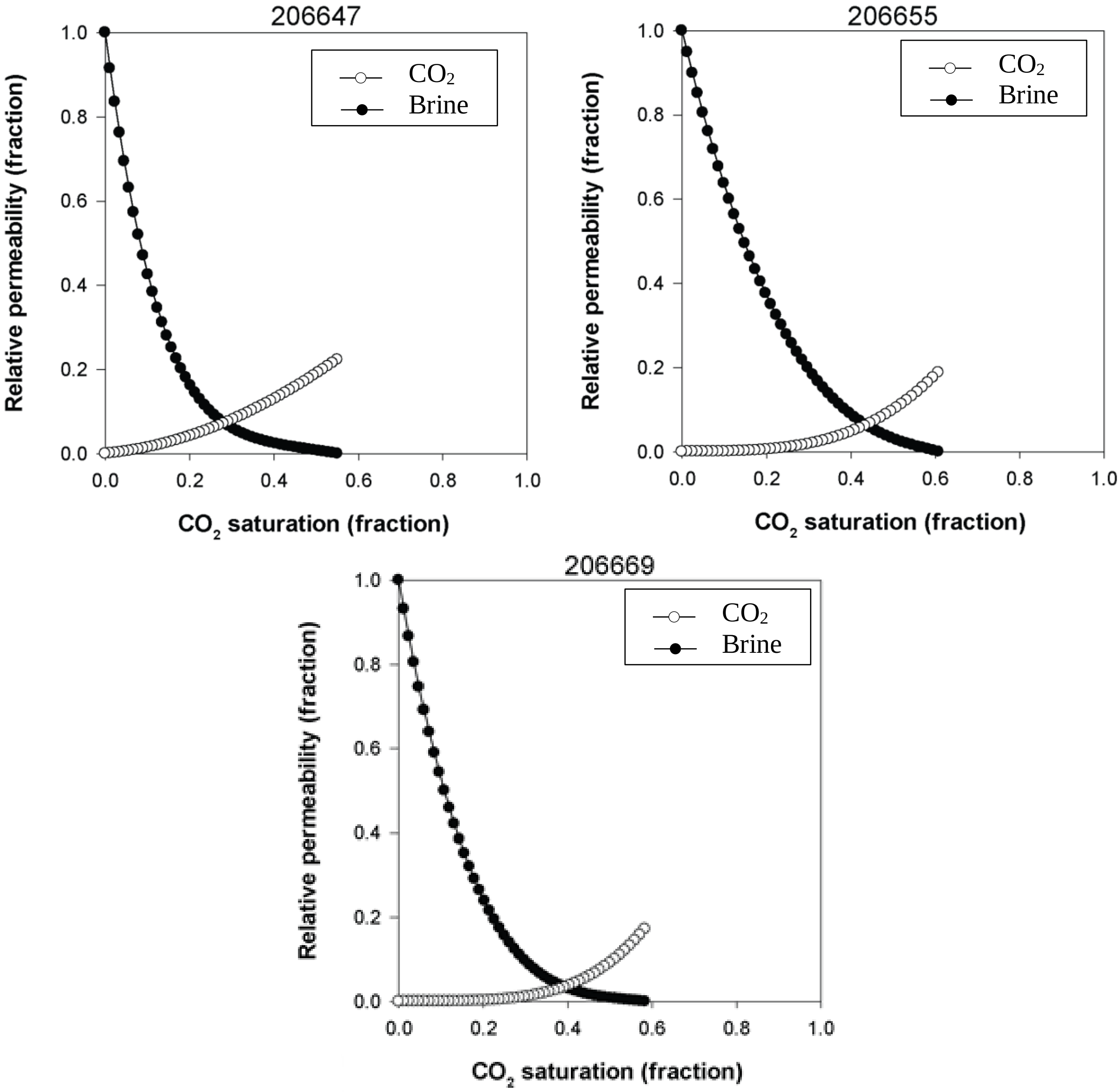

Figure 5. Relative permeability curves for the primary drainage conducted on the four samples.

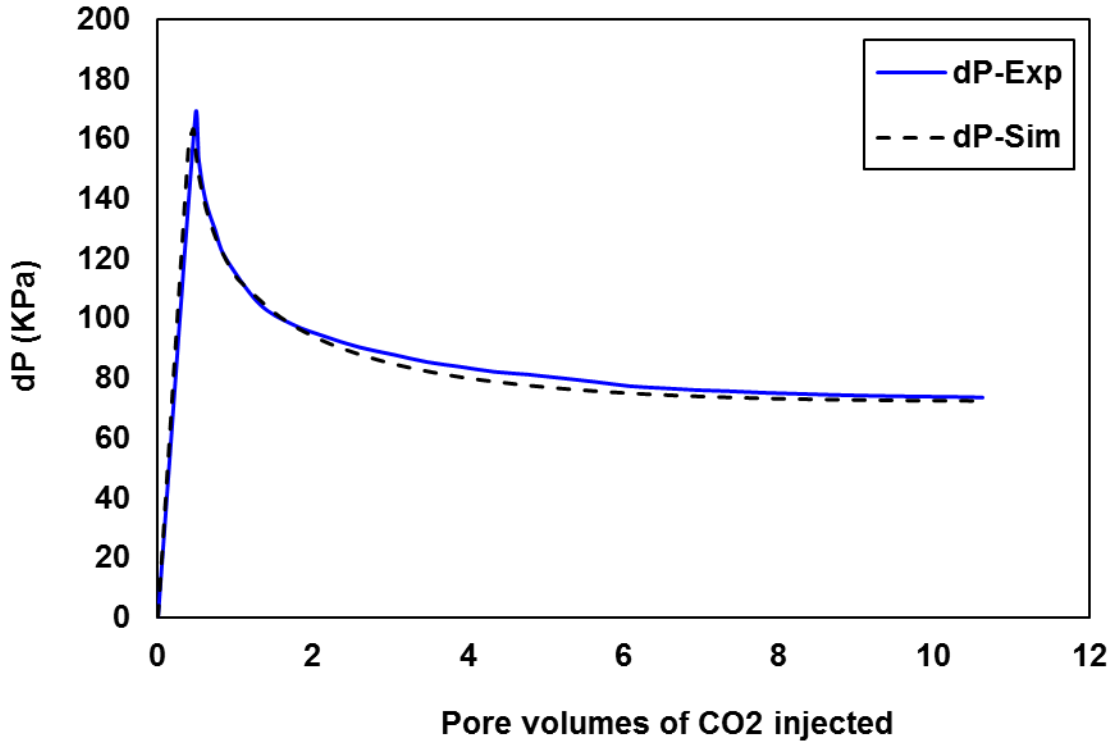

Figure 6. Comparison between the differtial pressure profiles for Sample 206655: blue: experimental data (used in Sendra software), black: numerical siulation results (Eclipse software (Schlumberger)).

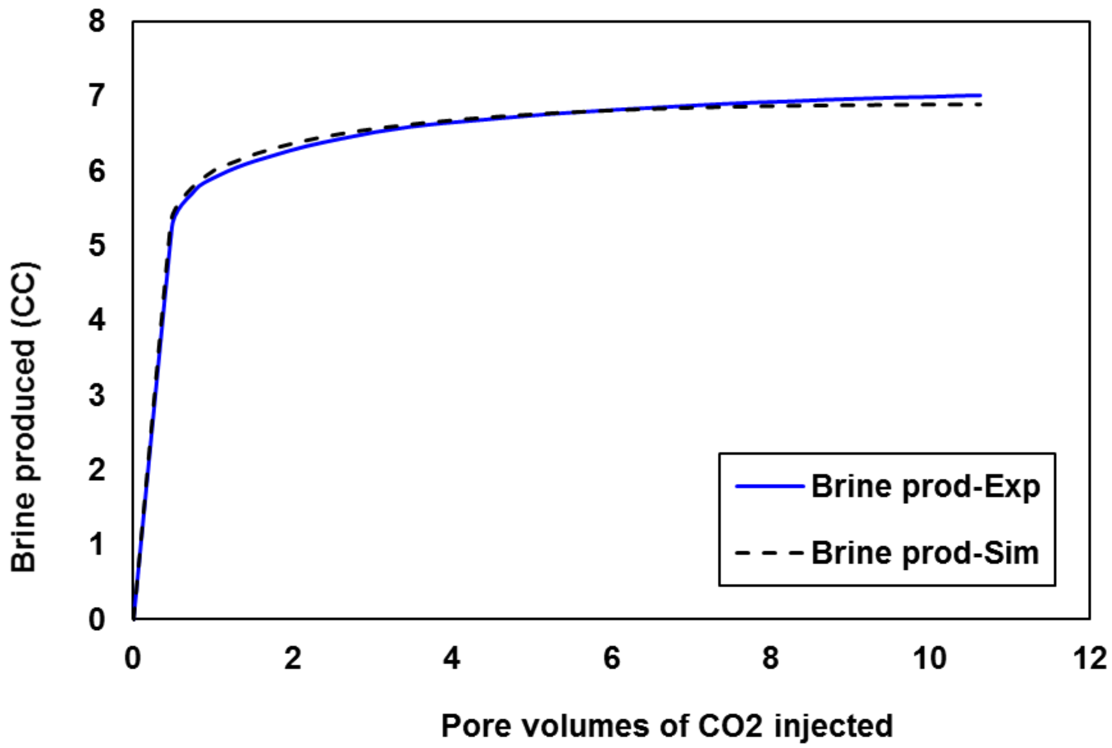

Figure 7. Comparison between the brine production profiles for Sample 206655: blue: experimental data (used in Sendra software), black: numerical siulation results (Eclipse software (Schlumberger)).

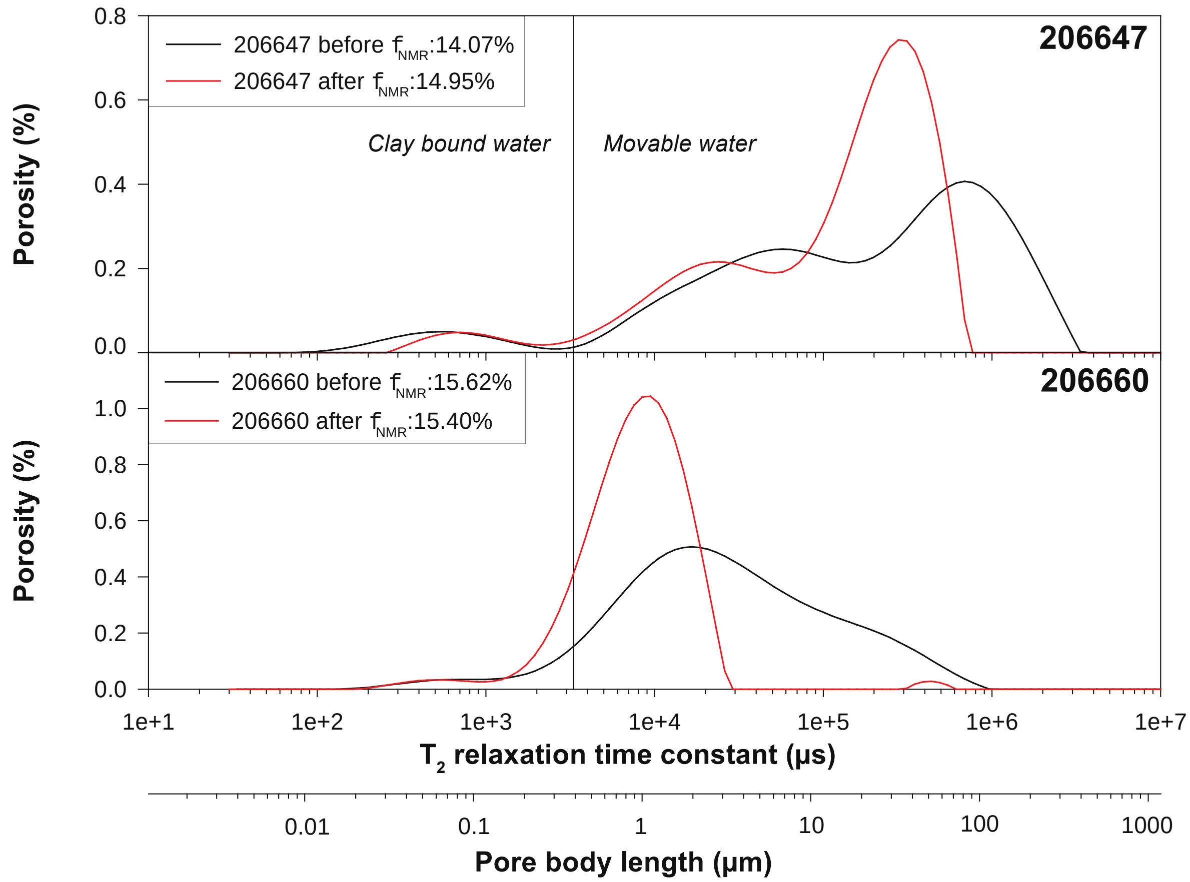

Figure 8. NMR T2 relaxation time distribution for two samples before and after core-flooding experiments. The total porosity is almost not affected by the flooding tests but the relaxation time curve for the same sample is signifciantly different..

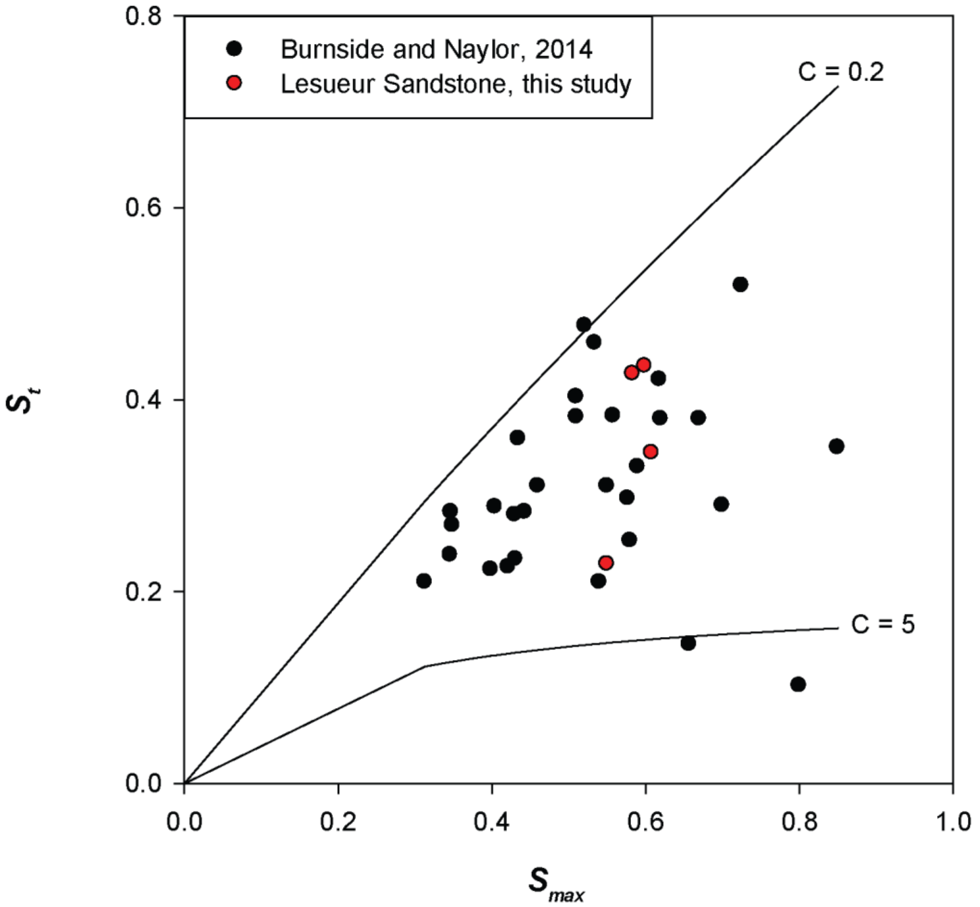

Figure 9. Scatter plot of residual (S_t) versus initial CO_2 saturation (S_{max}) obtained during core flooding experiments. Black dots represent sandstone related experimental data available in the open literature synthesised in the review from Burnside and Naylor, 2014. Continuous lines represent Land's model curves with trapping coefficient (C) of 0.2 and 5.

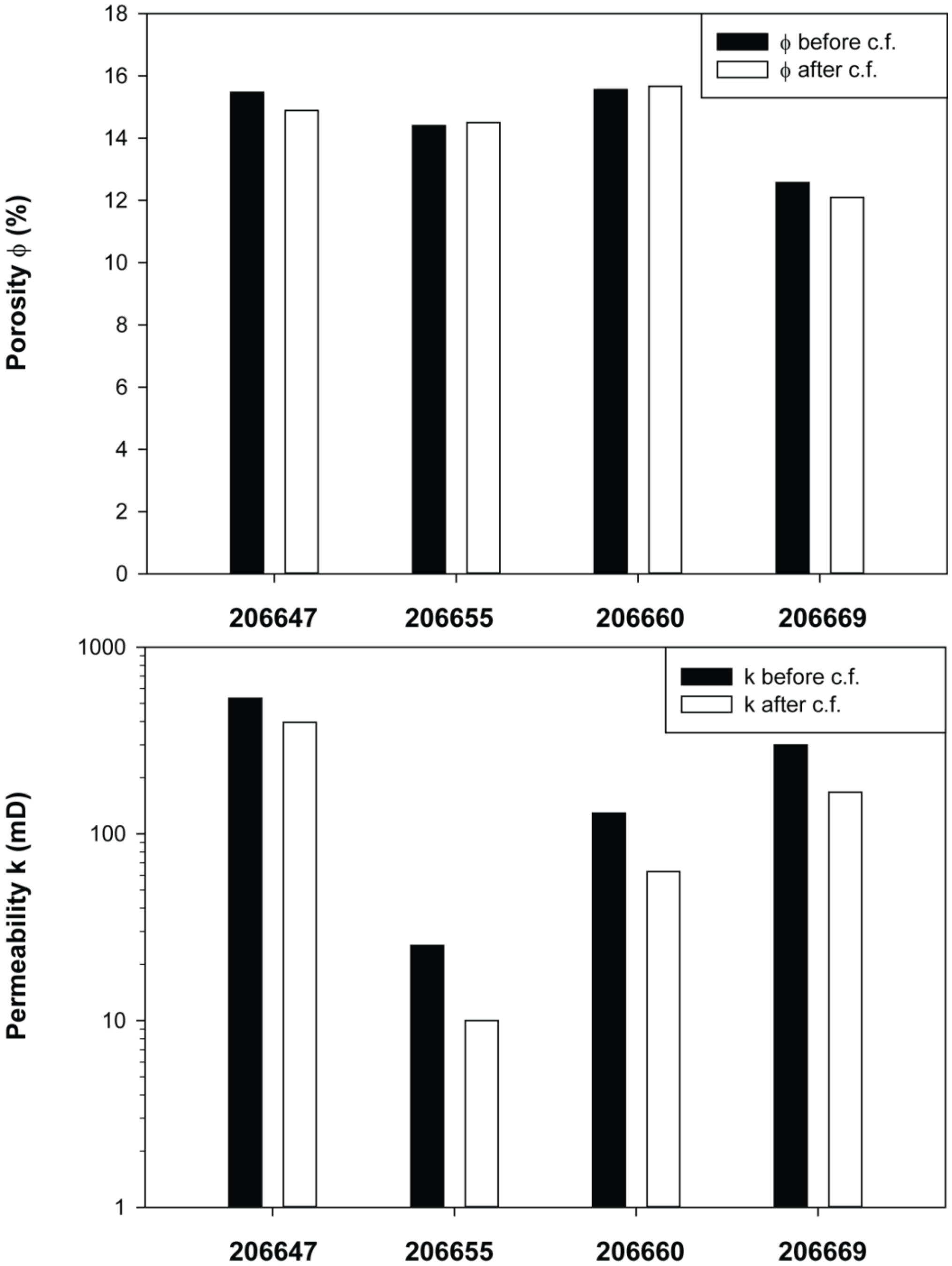

Figure 10. Porosity (Top) and gas permeability (Bottom) measured using the helium on four core plugs before and after core flooding experiments. Note that while the variation in posorisy in minimal, there is a significant decrease in permeabilty of all four sample.

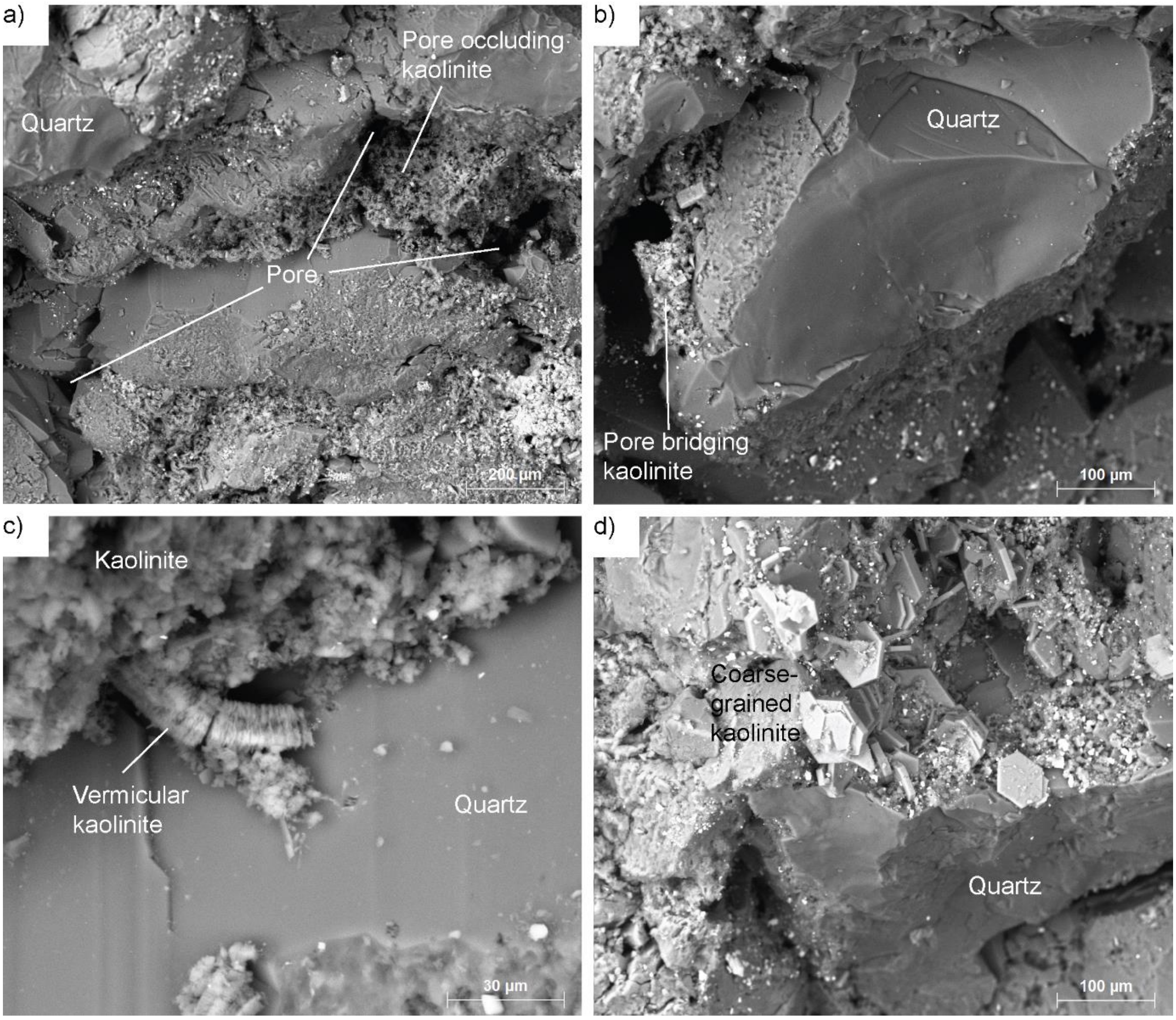

Figure 11. SEM images of sample 206669 showing the occurrence of diagenetic, kaolinite (Kaol in the figure) partially occluding the pores between detrital quartz grains (a); bridging pores between detrial grains (b). (c) vermicular diagenetic kaolinite growing on a quartz crystal surface. (d) well crystallized coarse-grained kaolinite.

Table 1. Reservoir P-T conditions during the experiment on the four core-plugs.

Reservoir parameter	Sample ID			
	206647	206647	206660	206669
Depth, m	1,901.6	1,927.0	1,935.5	2,491.6
Pore pressure (MPa)	19.05	19.06	19.39	24.95
Overburden pressure (MPa)	43.02	43.59	43.78	56.36
Reservoir temperature (°C)	60.7	61.0	61.2	69.2
Formation water salinity (ppm NaCl)	30,000	30,000	30,000	30,000

Table 2. Characteristics of the core-plugs used for the experiments and XRD derived mineralogy (in weight %). No XRD data is available for core-plug 206655. He ϕ = helium porosity; He k = helium permeability; Qz = quartz; K-feld = K-feldspar; Kaol = kaolinite; Ank = ankerite.

Sample ID	Depth (m)	He ϕ (%)	He k (mD)	Hg ϕ	Brine k (mD)	Qz	K-feld	Kaol	Ank
206647	1,901.6	15.47	532	16.73	48.0	86	10	4	-
206655	1,927.0	14.33	25		4.65	N/A	N/A	N/A	N/A
206660	1,935.5	15.56	129	16.38	16.5	77	12	7	4
206669	2,491.6	12.57	299	12.54	238	90	8	2	-

Table 3. End-point residual saturations and relative permeabilities.

Sample ID	**End-point Residual Saturation of the Displaced Fluid, %**			**End-point Relative permeabilities for the Displacing Fluid, fraction**		
	Primary Drainage	**Primary Imbibition**	**Secondary Drainage**	**Primary Drainage**	**Primary Imbibition**	**Secondary Drainage**
206647	45.00	22.87	44.22	0.223	0.353	0.230
206655	39.2	43.5	-----	0.188	0.25	-----
206660	40.12	42.71	-----	0.206	0.125	-----
206669	41.65	34.47	41.84	0.172	0.096	0.15

Table 4. Best-fit relative permeability parameters for core–floods fit to the Sigmund and McCaferry (1979) model

Sample ID	**N_w**	**N_g**	**A**	**B**
206647	**4.6335**	**1.9109**	**0.0895**	**0.2336**
206655	**2.8124**	**3.3497**	**0.1581**	**0.0051**
206669	**3.5880**	**4.1398**	**0.0538**	**0.0018**

Table 5. Rock and fluid properties used to construct the numerical model for Sample 206655 in Eclipse.

Fluid properties		
Fluid	**Density, kg/m^3**	**Viscosity, Pa.s**
$scCO_2$	705	0.58×10^{-4}
Brine	1010	4.8×10^{-4}

Rock properties	
Permeability, mD	**Porosity, %**
4.65	14.3

Table 6. Porosity and permeability measurements on pre- and post-core flooding experiments from the four core-plugs using helium and NMR methods. He ϕ = Helium porosity; NMR ϕ = NMR porosity; He k = Helium permeability; b.f. = before flooding; a.f. = after flooding.

Sample ID	He ϕ b.f. (%)	He ϕ a. f. (%)	NMR ϕ b. f. %	NMR ϕ a. f. (%)	He k b.f. (mD)	He k a. f. (mD)
206647	15.47	15.87	14.07	14.95	532	464
206655	14.33	14.4	-	-	25	10
206660	15.56	16.4	15.62	15.4	129	72
206669	12.57	12.75	11.95	-	299	188

Table 7. Initial CO_2 saturation (S_{max}), residual CO2 saturation (S_t), percentage of residually trapped CO2 (R) and Land's trapping coefficient C for the Lesueur Sandstone sample tested in this study

Sample ID	S_{max} (-)	S_t (-)	R (S_t/S_{max}) %	C (%)
206647	0.55	0.23	41.58	2.55
206655	0.60	0.44	72.62	0.63
206660	0.58	0.43	73.20	0.63
206669	0.61	0.34	56.69	1.26